ISSN: 0067-2904

Hyperspectral Image Sharpening Using Fusion Techniques -A Case Study at Salah Al-Din Province/Iraq-

Rawnak Adel Abdulwahab[1], Firas A. Hadi[2*]
[1]*Ministry of science and technology, Remote Sensing Centre, Baghdad, Iraq*
[2]*Dpt. of Renewable Energy Science, College of Energy and Environmental Science, Al-karkh University of Science, Baghdad, Iraq*

Received: 28/6/2022 Accepted: 25/12/2022 Published: 30/3/2024

Abstract

The data fusion process includes merging two or more pieces of information obtained from different sensors. Satellite image fusion research aims to create a new image by combining two images captured by different sensors using various methodologies. In this research, image sharpening tools were used to combine a hyperspectral image with a low spatial resolution captured by a Hyperion sensor mounted on the Earth Observation 1 (EO-1) satellite with a grayscale high spatial resolution image captured by Enhanced Thematic Mapper Plus (ETM +) sensor mounted on Landsat-8 (resampling first one to ensure equal spatial resolution of both images). In addition, three techniques were adopted for implementing the Fusion mechanism: the Principal Component Analysis PCA, the Nearest Neighbor Diffusion NNDifuse, and the Gram-Schmidt method; these were used to sharpen hyperspectral data using high spatial resolution. The result showed that the Gram-Schmidt method could give Hyperspectral images with higher spectral and spatial resolution in panchromatic image data more accurately than the other methods.

Keywords: Hyperion, hyperspectral, image processing, Image Fusion, Resolution.

تحسين الدقة المكانية للصور الفائقة الدقة الطيفية باستخدام تقنيات التوحيد

رونق عادل ، فراس عبد الرزاق
[1]وزارة العلوم والتكنولوجيا، مركز الاستشعار عن بعد، بغداد، العراق
[2] علوم الطاقة المتجددة، كلية علوم الطاقة والبيئة، جامعة الكرخ للعلوم، بغداد، العراق

الخلاصة

تتضمن عملية دمج البيانات دمج اثنتين أو أكثر من المعلومات التي تم الحصول عليها من أجهزة استشعار مختلفة. الهدف من أبحاث دمج صور الأقمار الصناعية هو إنشاء صورة جديدة من خلال الجمع بين صورتين تم التقاطهما بواسطة مستشعرات مختلفة باستخدام منهجيات مختلفة .في هذا البحث ، تُستخدم أدوات زيادة حدة الصورة من خلال الجمع بين صورة Hyperspectral مع دقة مكانية منخفضة تم التقاطها بواسطة مستشعر Hyperion المركب على القمر الصناعي Earth Observation 1 (EO−1) مع صورة ذات نطاق رمادي عالية الدقة تم التقاطها بواسطة مستشعر Enhanced Thematic Mapper Plus (ETM+) المثبت على

*Email: aFiras.A.Hadi@kus.edu.iq

القمر الصناعي لاندسات 8 (إعادة التشكيل الأول لغرض ضمان دقة مكانية متساوية لكلتا الصورتين). بالإضافة إلى ذلك ، تم اعتماد ثلاث تقنيات لتنفيذ آلية الدمج الصوري ، وهي طريقة PCA وطريقة انتشار الجار الاقرب NNDifuse وطريقة جرام شميدت Gram–Schmidt، تُستخدم كل هذه الطرق لصقل البيانات الفائقة الطيفية باستخدام دقة مكانية عالية. أظهرت النتائج أن طريقة جرام–شميدت يمكن أن تعطي صورًا فائقة الطيف ذات دقة طيفية أعلى بالإضافة إلى دقة مكانية عالية أفضل من الطرق الأخرى باستخدام بيانات الصورة احادية الطيف panchromatic.

1. Introduction

The image fusion method had proposed for the hyperspectral (HS) and panchromatic (PAN) combination using an adaptive tensor with a multi-scale Retinex algorithm, Jiahui *et al.* 2020. In their proposed method, an adaptive tensor-based method was presented to extract HS structure information effectively, and a multi-scale Retinex algorithm was introduced to obtain PAN's spatial and structure details. Jamila *et al.* 2021 proposed a variational fusion model with a nonlocal regularization term that encodes patch-based filtering conditioned to the geometry of the multispectral data. They further incorporated a radiometric constraint that injects the high frequencies of the scene into the fused product with a band-per-band modulation according to the energy levels of the multispectral and hyperspectral images. Leping *et al.* 2022 implemented the fusion by decomposing HS and multispectral (MS) images into simple image fusion tasks through a spectral grouping strategy. Using existing image fusion algorithms, HS, MS, and PAN images were fused step by step. According to different fusion orders, two strategies ((HS+MS)+PAN and HS+(MS+PAN)) were proposed using simulated and real Gaofen-5 (GF-5) HS, MS, and PAN images from the Gaofen-1(GF-1) sensors as experimental data [1] [2] [3] .

The hyperspectral imaging sensor can collect tens or hundreds of spectral bands in a wide coverage range. Materials often have different reflectance for different wavelengths, so a hyperspectral image enables accurate identification of different materials due to its high spectral resolution and wide range.

Due to the high spectral resolution, hyperspectral images provide a wide range of spectral detail for precise land feature analysis. However, the limitations of sensors could cause images to have a low spatial resolution. Thus, increasing tidal resolution became essential in encouraging fusion technology to produce improved HS data that contributes to accurate spatial images [4] [5].

Image fusion technology represents a set of methods and tools that adopt data from multiple sources and carry a different nature to increase information accuracy and quality. Figure1 gives an idea of the hyperspectral image fusion process, where low spatial resolution hyperspectral images are combined with high-resolution broadband (grayscale) images to produce high-resolution hyperspectral spatial resolution images. Increased information quality means the post-merge signal contains more helpful information than the original signal. That, in turn, means new information has been added to the original signal during the merging process. The goal of the fusion technique, in general, is to collect complementary information. The merging technique can obtain scenes with better spatial and spectral accuracy based on two different spatial and spectral images. Combining multiple same-scene images provides different information because each image was captured with a different sensor. The high spectral

resolution allows the scene to determine the material quality, while the high spatial resolution determines the location of those materials [6].

All remote sensing images have a specific spatial resolution and spectral resolution limit, besides no ideal sensitive sensor to whole spectral wavelengths that produce spatial data. However, the image captured by a particular sensor may complement the images from different sensors. For example, a new satellite imaging system, including Landsat 8 (ETM +) and EO-1 Hyperion Hyperspectral imagery, produces two sets of image data, one with high spatial resolution without spectral bands. In contrast, the other with low spatial resolution consists of many spectral bands [7].

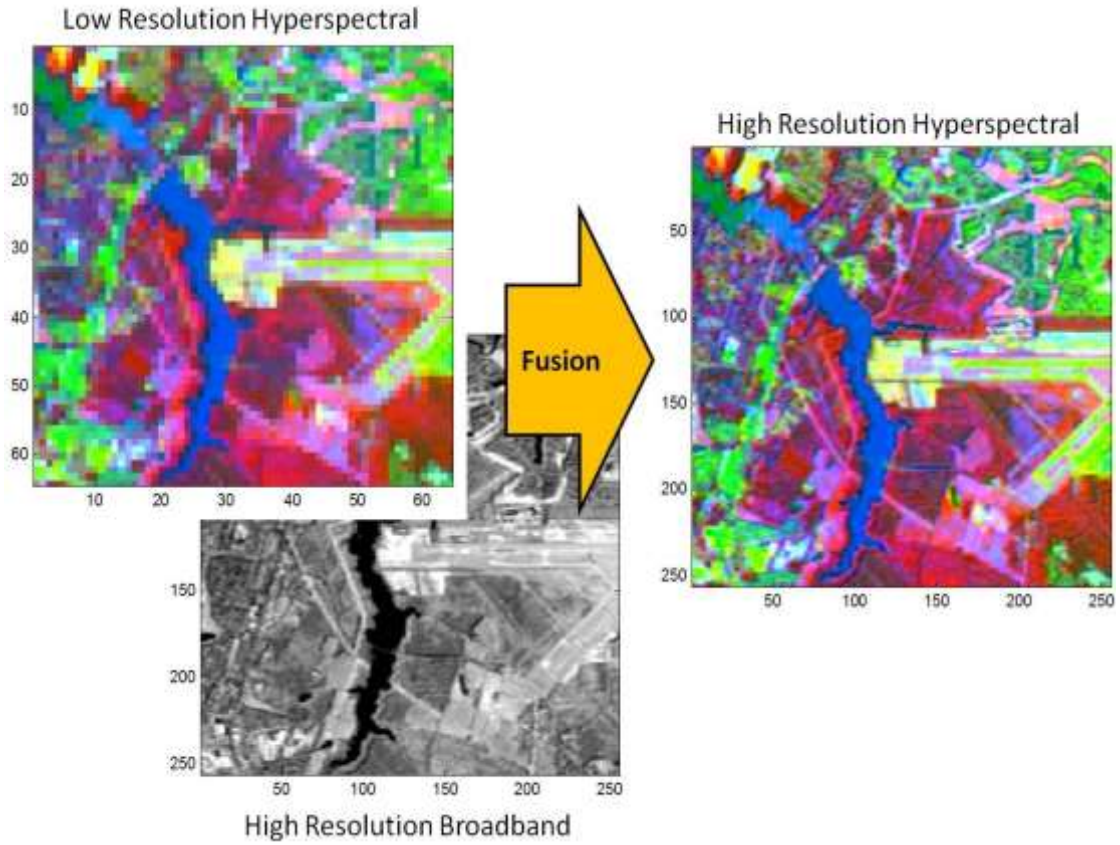

Figure 1: High-resolution spectral picture and a high-resolution spatial image are fused, and a hyper-resolution spectral and spatial image is produced.

2. Hyperion

Hyperion is a push broom sensor type with one spectrometer and one telescope. The EO-1 satellite has a synchronous orbit with the sun at an altitude of 705 km, and it is one minute late to the Landsat-7 satellite. Hyperion sensor images have 256 pixels with a size of 30 m on the earth's surface on a 7.65 km swath. The platform's position can change when the satellite changes to new targets in the image. Hyperion processing was developed and refined in its first year of operation to a stage (Level 1-B1) such that the processing data becomes available. This research studied processing methods that can be applied to (Level 1-B1). Hyperion data has three advantages: First, it can provide improved atmospheric correction information to derive surface reflection. Second, it can provide easy access to spectral coefficients based on surface

reflection. Finally, Hyperion data can bin or integrate hyperspectral data into synthetic bands equivalent to either broadband sensors or device ranges that have not yet been developed [8].

3. Panchromatic Data

The panchromatic band range on the Landsat 8 Operational Land Imager (OLI) sensor (Band 8) covers a narrower spectrum portion than the corresponding band range in Landsat 7 ETM +: 0.50-0.68 micrometers (L8 OLI) in contrast to 0.52-0.90 micrometers (L7 ETM +). The band-8 (panchromatic) resolution appears at 15 meters in black and white see Figure 2.b., and captures a much more comprehensive range of light than other bands. Therefore, it provides a more precise and detailed picture twice as detailed as the individual spectral bands; Figure 2. a gives an idea of the images from the Hyperion and OLI sensors.

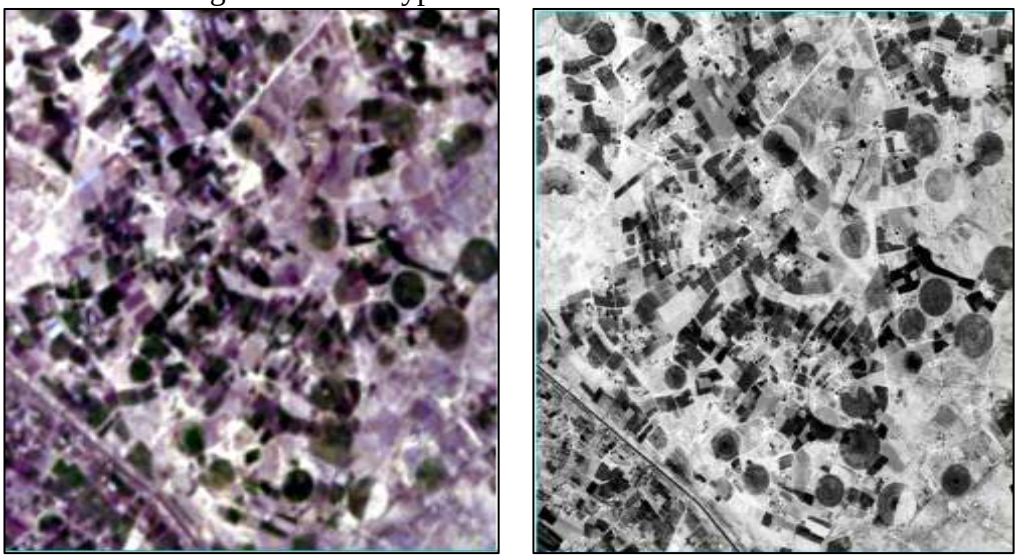

a- Hyper Spectral b- Panchromatic image

Figure 2: The base images used in this research

4. Materials and Method

4.1. Data Acquisition

The study area is located South of Salah Al-Din province in the northeast of Iraq with a geographical coordinate of 43.885686 Longitude, 34.316930 Latitude, and 74m Elevation, Figure 3. The northern region of the Iraqi province is depicted in the landscape on the left, and the arrow points to the study area. However, the view on the right depicts an extended portion of the selected study site.

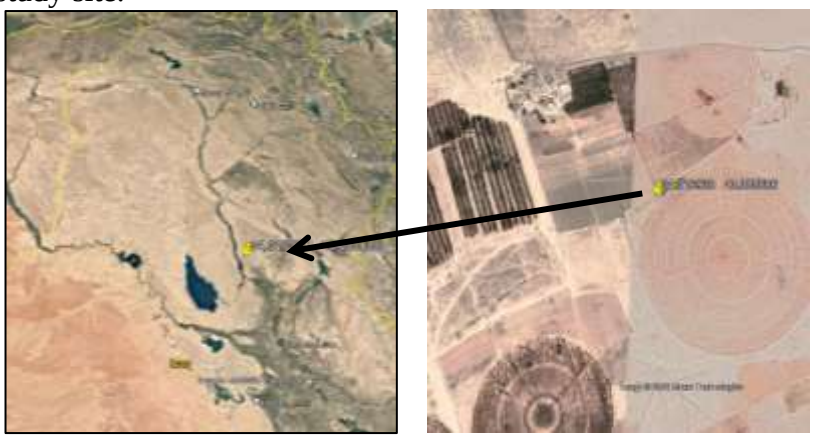

Figure 3: The area of study, which is located South of Salah Al-Din, Iraq

4.2. Hyperspectral Bands

There are 242 bands in Hyperion data ranging from 355nm to 2577nm; the Visible and Near-Infrared (VNIR) detector gathers data from 1 to 70 bands, while Short-Wave Infrared (SWIR) detector gathers data from 71 to 242 bands. Only 198 of the 242 bands in the Level 1 radiometric product are calibrated. There are only 196 distinct channels because the VNIR and SWIR focal planes overlap. The VNIR and SWIR calibrated channels are 8–57 and 77–224, respectively. The detector's poor responsiveness was mainly blamed for the failure to calibrate all 242 channels. In specific channels, the uncalibrated bands are set to zero. The Level-1 product's digital values are recorded as a 16-bit signed integer and 16-bit radiances [9].

4.3. Removal of Absorption Bands and No Information Bands

During Level 1 processing, some bands were set to zero; these bands are (1-7), (58-76), and (221-242), and the remaining are 192 bands. Among the 192 unique ranges, several atmospheric water vapor bands absorb most of the solar radiation, which was determined by studying the radiance spectra. During the analysis of the hyperspectral images, it is found that the strongest vapor water bands seen between 1346 nm (band120), 1497 nm (band135), 1517 nm (band137), 1537 nm (band139), and 568 nm (band142), 1578 nm (band 143), 1598 nm (band145), 1669 nm (band 152), 1689 nm (band 154), 1709 nm (band 156), 2385 nm (which is band 213). All those proceeding bands have no or little information that can be ignored for further subsequent processing. However, some atmospheric correction programs like ENVI FLAASH need bands centered near 1380 nm in potent water vapor to clouds mask (high clouds). Therefore, bands (123-125) and wavelengths (1376 nm, 1386 nm, and 1396 nm) are saved in the image. As mentioned above, the strong water vapor bands were ignored in addition to zero bands, leaving a subset of about 92 bands that used atmospheric correction and other treatments. Zero and strong water vapor bands were rated "bad" and ignored in subsequent processing to reduce data volume and speed up processing [10].

4.4. Removing Damaged Vertical Stripes and Columns

It is essential to know that Level R1 consists of the number of bad bands affected by vertical stripes, which were reduced by replacing the value of Digital Number (DN) for the affected column with the values of average DN for adjacent columns [10].

4.5. Atmospheric Correction

Atmospheric correction is an essential step before processing. This study attempts to reduce the effect of atmospheric correction on the study area's hyperspectral bands and time, monsoons, clouds, and much water vapor in the atmosphere. There is also a spectral variation in the vegetation cover of the region in its total activity.

Aerial Hyperion image correction is an essential step. The FLAASH model was used for atmospheric correction to convert image radiance values to reflection values [11].
FLAASH is a technique used to correct image errors caused by the atmosphere's influence as it works to correct wavelengths starting from the visible area, near-infrared, and short waves in the infrared, reach to 3μm. It is essential to know that unlike many programs designed to correct the effects of the atmosphere that deals with the database of transmitted radiation properties and before calculating the results, FLAASH includes the MODTRAN4 code for transmitting radiation. The effect of both water vapor and aerosols can only be restored when the scene consists of proper wavelength location bands. Images that contain geometric errors, such as

vertical (nadir) or slant viewing (off-nadir) geometry, can be corrected using FLAASH technology. FLAASH technology could be summarized as follows [11]:

- Repair the adjacency effect (pixel mixing due to the scattering of the reflected radiation on the surface).

- Step of calculating the average view of the scene to remove aerosols and fogging effect, where FLAASH uses advanced technologies to address weather conditions.
- Processing a delicate and dark cloud classification map.
- Artifact suppression step, which makes spectral polishing.

4.6. Geometric Correction

A georeferenced Hyperion image was obtained from the USGS; the image was used as a reference scene, which will be used to match the unrectified scene. The projection is UTM at Zone 38(North) and Datum: WGS84. GCPs were identified on the reference scene, and the original images for mathematical modeling were used to eliminate geometric distortion presented in the unrectified image [11].

4.7. Interpolation and Resampling

These operations involve extracting pixels values (chromatic brightness) from a position in the original input image (distorted) and putting them into a suitable coordinate position by which the output image is corrected; the processes of resampling, namely (Bilinear Interpolation, Nearest Neighbor, and Cubic Convolution). The last one was applied for our interpolation processing [11].

4.8. Fusion Techniques

In this research, three fusion techniques were adopted in order to get a fused output image:

4.8.1. Principal Component Analysis (PCA) for Image Fusion

The principal component analysis fusion method can be performed by replacing the normalized brightness high-resolution scene with the 1st PCA (i.e., PCA1), and then the inverse PCA transform is performed as illustrated in the block diagram shown in Figure4.

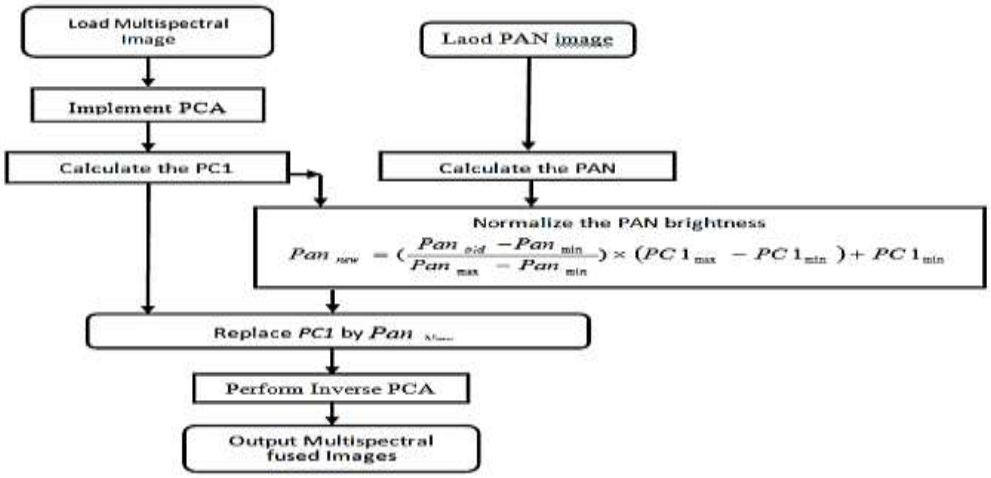

Figure 4: The block diagram illustrating the procedures involved in the PCA fusion method

This technique has been implemented on hyperspectral images to produce PC1, PC2, and PC3.., replace PC1 with PAN image, then inverse PCA transform to obtain a fused image.

4.8.2. NNDiffuse Panchromatic Sharpening

If the spectral response function of each hyperspectral band has minimum overlapping value with one another, then the NNDiffuse pan-sharpening process will work well, such that the components of all hyperspectral bands contain the spectral range of the panchromatic raster. The following could summarize the requirements for running the NNDiffuse panchromatic sharpening algorithm:

- The pixel dimension (size of a pixel) of the low-resolution raster (hyperspectral) data must be equal to multiple integers of the pixel dimension (pixel size) of the high-resolution raster data (panchromatic); if this condition is not met, a preprocessing step must be performed, including resampling low-resolution raster data [12].
- Each panchromatic raster must have the same projection; geometric correction must be applied if not.
- The hyperspectral raster must be aligned; if not, registration must be done.

4.8.3. The Gram-Schmidt pan-sharpen method

The method depends on computing a simulated low-resolution Pan band as a linear combination of the MS bands:

$$pan_{sim} = \sum_{k=1}^{n} w_k MS_k \quad \ldots\ldots\ldots\ldots\ldots\ldots\ldots\ldots\ldots\ldots\ldots\ldots \text{(1)}$$

Where,
Pan_{sim} = low-resolution Panchromatic band,
w_k = MS to Pan weights,
MS_k= multispectral bands
n=number of bands

By manipulating each band and then starting simulating the band such as the first vector, making the whole ranges perpendicular using the orthogonal Gram-Schmidt feature; for Gram-Schmidt Pan-sharpening, each of the incoming differences was made free of direct current first (get their means); the iterative procedure remains the same [12] [13].

5. Results and Discussions

One of the most cutting-edge technologies today is the utilization of hyperspectral satellite imagery, which is regarded to be a revolution in the field of remote sensing both globally and in Iraq specifically. Applying these approaches and studies to Iraqis' images is novel and unfamiliar; the spatial accuracy of this sort of image has been enhanced while keeping the spectral accuracy to the greatest extent.

- **Atmospheric Correction**

The image bands must be resized to 48, besides using the FLAASH model. The following entries were considered starting from the location of the study area, satellite sensor type, date of flight, sensor's altitude, and mean ground elevation ending with the time of flight; all of them were used as inputs for processing the radiance data.

Optionally, to obtain more valuable and accurate correction results, the tropical atmospheric and maritime aerosol models were selected, also the information on water vapor content extracted from the water absorption bands of Hyperion.

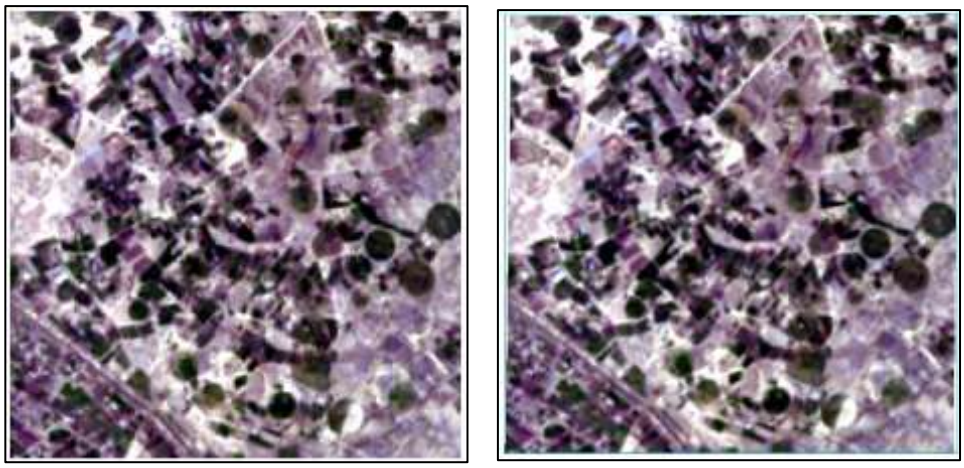

(a) Original Band (b) After FLAASH Correction

Figure 5: Hyperspectral images of the study area

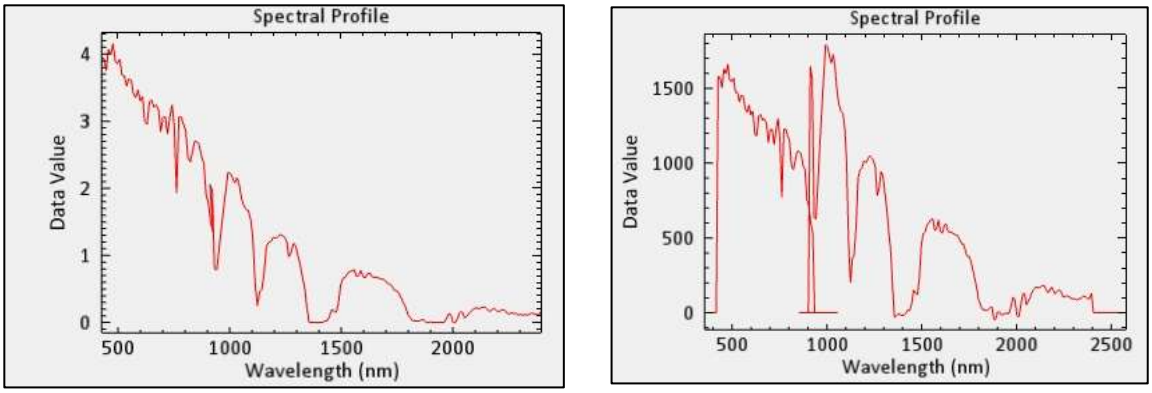

(a) Original data (b) After FLAASH Correction

Figure 6: Spectral graph of the study area

Figure 5 shows the characteristics' differences before and after applying the atmospheric correction model. There was no visually clear difference after applying the FLAASH model. Statistically, this can be explained by seeing the spectral profile shown in Figure6 (change of wavelength versus reflection value) before and after applying the FLAASH model. Part of this research is about vegetation, as this appears clear through the visible part of the spectrum, as the chlorophyll layer in plants absorbs waves that fall within the red and blue wavelengths more strongly than the wavelengths that fall within the green color. This results in a small reflective spectrum peak that falls within the green wavelength range, which can be observed in Figure 6 (b) after correcting the FLAASH model. Then, the reflection spectrum rises clearly across the boundaries between the red wavelengths, which lie close to the infrared spectrum, mainly due to the cause of interactions with the leaves' internal cellular structure [9].

From the graph above, an observed improvement in the vegetation feature category after running both models was observed; the lateral tilt between wavelengths (625 to 750) and in the range of 875-1000nm decreases after atmospheric FLAASH correction. On the other hand, an

increase in the values starting from the blue region and a steep slope in the air-corrected profile was observed. Also, several narrow peaks in wavelength from 750 to 1500nm can be observed from the air-corrected image file. It was also observed that the correction results in the near-infrared region appeared better after FLAASH correction.

- Fusion techniques

Figure 7a represents a selected Hyperion EO-1 satellite section for the Salah Al-Din province image. Figures 7b-d show the hyperspectral images after applying PCA, NDDifuse, and Gram-Schmidt with PAN image fusion methods. After applying the fusion techniques, figures 8-10 show the soil, vegetation, and highway spectral profile. Subjectively, it is obvious how Gram-Schmidt is superior to the other methods in its ability to preserve the edges of the image

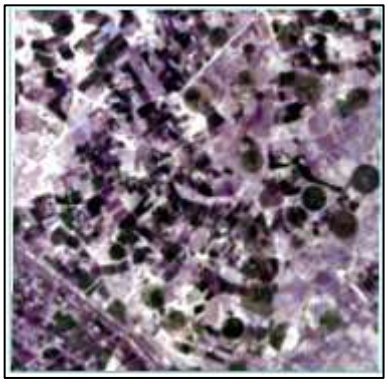

(a) Hyperspectral Base Image

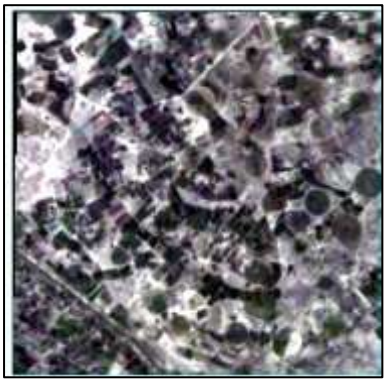

(b) PC image fused

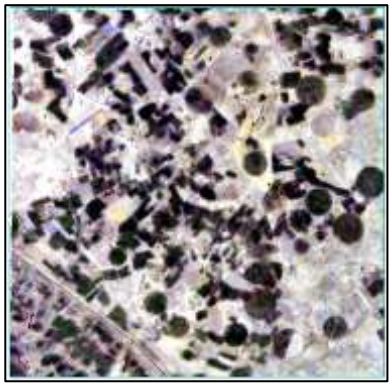

(c) NDDifuse image fused

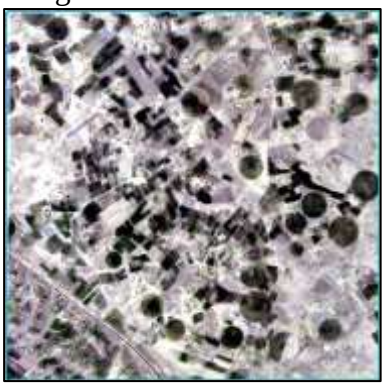

(d) Gram image fused

Figure 7: (a) Hyperspectral image (b, c, and d) resultant Fusion images

Figure 7 shows the subjective comparison between the three previous techniques. In addition, it is necessary to know the extent of the superiority of the three methods in applying the fusion technique objectively. Thus, after applying fusion techniques, figures 8-10 show the soil, vegetation, and highway spectral profile. Comparing the spectral profile of the base image with the images resulting from the fusion process using three methods produced a possibility to notice that the spectral representation of both NDDifuse and Gram-Schmidt have a good match with the base representation.

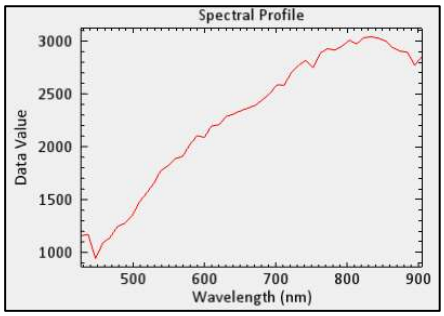

(a) Soil spectral profile for base image

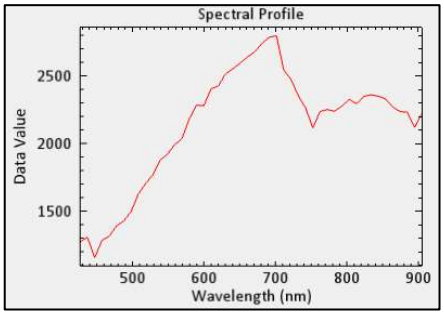

(b) PC image fused

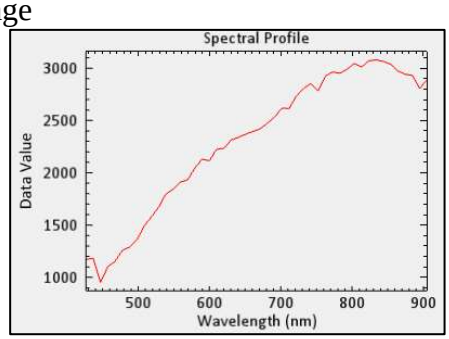

(c) NDDifuse image fused

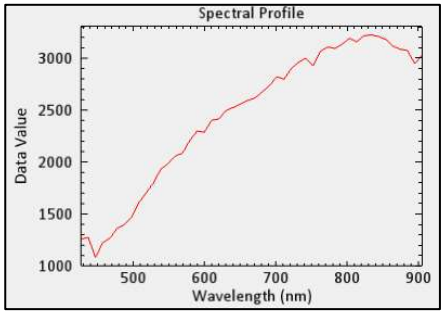

(d) Gram image fused

Figure 8: Soil spectral profile in the hyperspectral image (a) for base image (b, c, and d) for fusion resultant images.

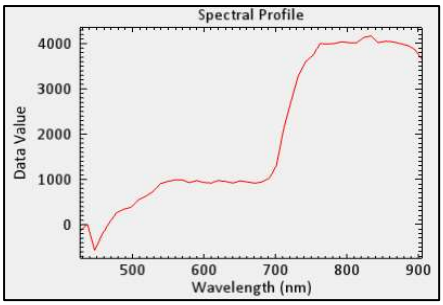

(a) Vegetation spectral profile for base image

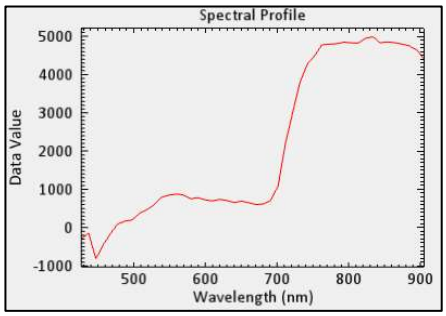

(b) PC image fused

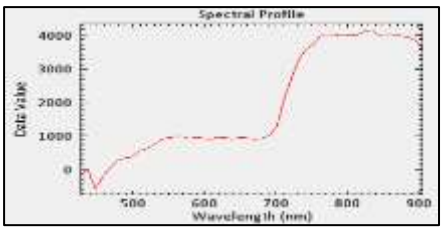

(c) NDDifuse image fused

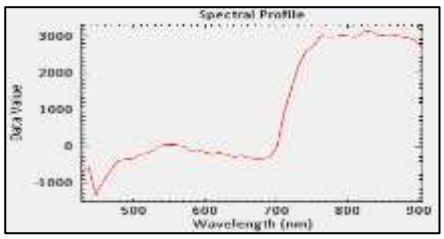

(d) Gram image fused

Figure 9: Vegetation spectral profile in the hyperspectral image (a) for base image (b, c, and d) for fusion resultant images.

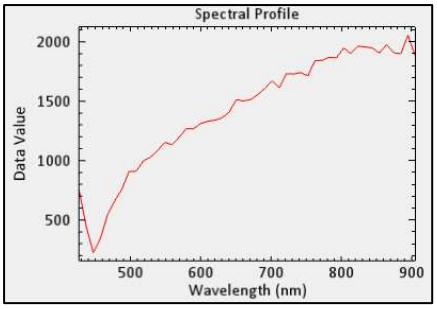

(a) Highway spectral profile for base image

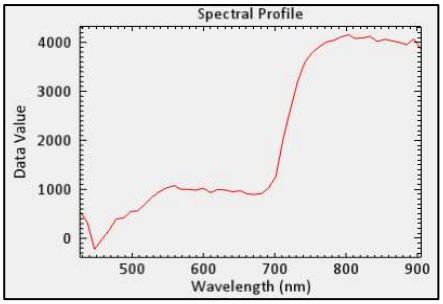

(b) PC image fused

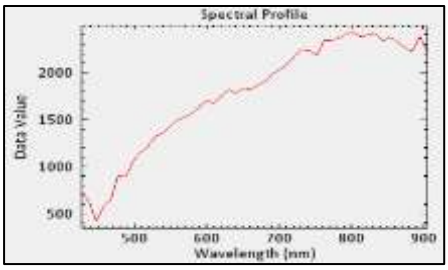

(c) NDDifuse image fused

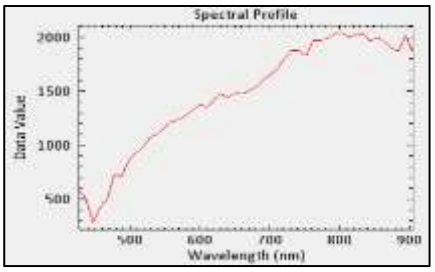

(d) Gram image fused

Figure 10: Highway hyperspectral image (a) base image (b, c, and d) for fusion resultant images.

Finally, the algorithm was applied to the Salah Al-Din image (EO1 hyperspectral 30m resolution) image fused with Landsat Panchromatic "PAN" (15m spatial resolution) using Principle Component Analysis to fuse the sample of the image illustrated in Figure11.

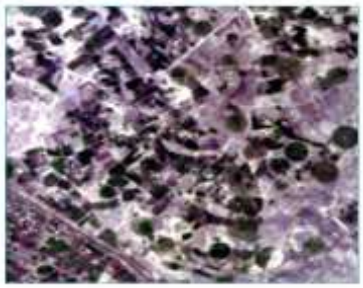

(a) EO1 Hyperion image 30m resolution

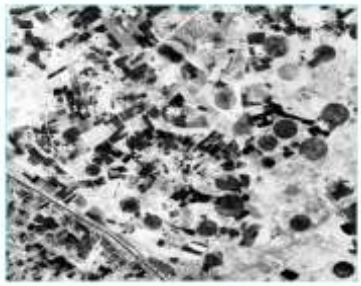

(b) Panchromatic Landsat image 15m resolution

(c) PC Fused image

Figure 11: (a) Original Hyperion image with image 30m resolution (b)Panchromatic Landsat image 15m resolution (c) resultant PC image.

Conclusions

After applying the FLAASH technology, the image haziness was reduced to a minimum value, while the features and brightness sharpness were increased. It is evident from the

characteristics of the spectral waves after the correction process that the strong absorption bands are located near VNIR and SWIR, and thus these properties and features have been compensated and corrected largely. From the results, it could be concluded that:

- Hyperspectral image sharpening using the fusion technique improves spatial and spectral resolution in an image.
- The Panchromatic image improves the spatial resolution of the Hyperspectral image from 30m to 15m.
- Hyperspectral image Sharpening using Gram-Schmidt and NNDifuse methods gives better results than the PC method.

References

[1] L. Huang, Z. Hu, X. Luo, Q. Zhang, J. Wang, G. Wu, "Stepwise Fusion of Hyperspectral, Multispectral and Panchromatic Images with Spectral Grouping Strategy: A Comparative Study Using GF5 and GF1 Images," *Remote Sensing,* vol. 14, no. 4, 2022.

[2] J. Mifdal, B. Coll, J. Froment, J. Duran, "Variational Fusion of Hyperspectral Data by Non-Local Filtering," *Mathematics,* vol. 9, no. 11, 2021.

[3] J. Qu, Y. Li, Q. Du, H. Xia, "Hyperspectral and panchromatic image fusion via adaptive tensor and multi-scale retinex algorithm," *IEEE,* vol. 8, pp. 30522-30532, 2020.

[4] X. u, D. Yang, F. Jia, Y. Zhao, "Coupled Convolutional Neural Network-Based Detail Injection Method for Hyperspectral and Multispectral Image Fusion," *Applied Sciences,* vol. 11, no. 1, p. 288, 2021.

[5] R. Dian, S. Li, B. Sun, A. Guo, "Recent advances and new guidelines on hyperspectral and multispectral image fusion," *Information Fusion,* vol. 69, pp. 40-51, 2021.

[6] N. Tran, R. Mankar, D. Mayerich, Z. Han. (2020). "Hyperspectral-Multispectral Image Fusion with Weighted LASSO," Available: http://arxiv.org/abs/2003.06944.

[7] C. Guilloteau, T. Oberlin, Q. Berné, E. Habart, N. Dobigeon, "Simulated JWST data sets for multispectral and hyperspectral image fusion," *The Astronomical Journal,* vol. 28, no. 1, p. 160, 2020.

[8] Q. Xie, M. Zhou, Q. Zhao, D. Meng, W. Zuo, Z. Xu, "Multispectral and hyperspectral image fusion by MS/HS fusion net," *Procee-Dings of the IEEE Computer Society Conference on Computer Vision and Pattern Recognition,* pp. 1585-1594, June 2019.

[9] P. Barry, EO-1/Hyperion science data user's guide, Level 1_B, Redondo Beach, CA, Rep. HYP. TO: Defense & Information Systems, 2001.

[10] DG. Stavrakoudis, E. Dragoz, IZ. Gitas, CG. Karydas, "Decision fusion based on hyperspectral and multispectral satellite imagery for accurate forest species mapping," *Remote Sensing,* vol. 6, p. 6897–6928, 2014.

[11] M. Gholoum, D. Bruce, SA. Hazeam, "Image Fusion Applied To Satellite Imagery for the Improved Mapping and Monitoring of Coral Reefs: a Proposal," *ISPRS - International Archives of the Photogrammetry, Remote Sensing and Spatial Information Sciences,* vol. 39, pp. 211-216, Jul. 2012.

[12] M. Al-Oraiqat, EA. Bashkov, V. Babkov, C. Titarenko, "Fusion of multispectral satellite imagery using a cluster of graphics processing unit," *International Geoinformatics Research and Development Journal,* vol. arXiv preprint arXiv:1803.00737, 2018.

[13] ST. Yaseen, AH. Shaban., "Detection of altered water content of AlHammar marshes," *AIP Publishing LLC,* vol. 2307, no. 1, 2020.